analytical chemistry

pubs.acs.org/ac Article

PEGylated Ni Single-Atom Catalysts as Ultrasensitive Electrochemiluminescent Probes with Favorable Aqueous Dispersibility for Assaying Drug-Resistant Pathogens

Yuchan Ma, Yu Zhang, Jiaqi Gao, Hui Ouyang, Yong He,* and Zhifeng Fu*

Cite This: *Anal. Chem.* 2022, 94, 14047−14053 Read Online

ACCESS | Metrics & More | Article Recommendations | Supporting Information

ABSTRACT: Ni single-atom catalysts (SACs) were synthesized by high-temperature calcination of nickel ions and 1,10-phenanthroline on carbon black as a carrier. Benefiting from the ultrahigh atom utilization efficiency, Ni SACs can significantly accelerate decay of dissolved oxygen to generate abundant reactive oxygen species through an oxygen reduction reaction occurring on cathodes. The generated reactive oxygen species can vastly enhance the electrochemiluminescent (ECL) signal of luminol without participation of exogenous co-reactants. To overcome the inherent unfavorable aqueous dispersibility of Ni SACs prepared by the calcination protocol, they were functionalized with highly hydrophilic PEG 2000. Thanks to the abundant carboxyl groups on PEG 2000, the PEGylated Ni SACs (Ni@PEG) can be used as ECL probes to tag biorecognition molecules. In this proof-of-principle work, an ECL biosensor for assaying methicillin-resistant *Staphylococcus aureus* was developed by using porcine IgG as capture molecule and phage cell-binding domain tagged with Ni@PEG as signal tracer. It shows a broad linear range of 73−7.3 × 10^6 CFU/mL and a low detection limit of 25 CFU/mL. The recovery values for assaying spiked samples are between 80.8 and 119.2%. It was also utilized to assess MRSA susceptibility to four antibiotics, with results consistent with those obtained by the standard broth microdilution technique. To the best of our knowledge, it is the first time to utilize aqueous dispersible SACs as highly sensitive ECL probes for developing biosensors.

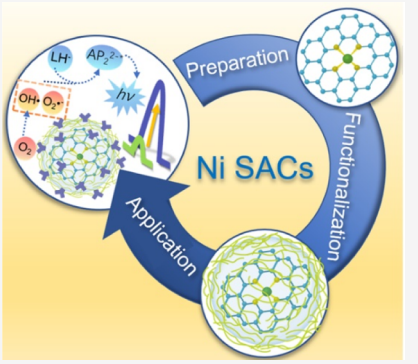

INTRODUCTION

The "superbug" methicillin-resistant *Staphylococcus aureus* (MRSA) is a widespread multidrug-resistant bacterium, which has already caused conspicuous morbidity and mortality.[1−3] Due to the urgency of this public health concern, it is a requisite to establish sensitive methods for assay and antimicrobial susceptibility testing (AST) of MRSA. Although bacterial culture-based protocols have long been the gold standard for bacterial assay and AST due to their satisfactory reliability, it is inevitably restricted by very long culture time.[4−6] PCR-based methods can shorten the assay time to 4−5 h but sometimes suffer from false results caused by exogeneous contaminants.[7−9] Recently, some molecular recognition-based methods using antibody, aptamer, and phage functional protein as biorecognition molecules have attracted increasing interest owing to their merits of rapidity, facileness, and reliability.[10−14] However, their sensitivity is obviously inferior to that of the traditional methods that rely on bacterial culture and PCR technique due to the absence of bacterial cell proliferation and nucleic acid amplification. Therefore, it is crucial to seek ultrasensitive signal probes for these molecular recognition-based methods to achieve comparable or superior sensitivity.

Electrochemiluminescent (ECL) assay has been extensively applied for drug safety, clinical diagnosis, bioimaging, and environmental monitoring, thanks to the advantages of satisfactory sensitivity, facile manipulation, and less reagent consumption.[15−17] The common ECL systems based on $Ru(bpy)_3^{2+}$ and quantum dots usually involve the participation of exogenous co-reactants such as tripropyl amine and $K_2S_2O_8$.[18,19] For some other ECL systems based on luminol,[20] MOFs,[21] and 3D porous g-C_3N_4,[22] dissolved oxygen acts as the essential co-reactant. In their ECL pathway, dissolved oxygen generates reactive oxygen species (ROS) through oxygen reduction reaction (ORR), which reacts with the ECL reagents or intermediates to emit ECL signal.[23] Due to the very limited efficiency of ORR, great efforts have been focused on exploring novel co-reaction accelerators (CRAs) to generate abundant ROS.[24−27] Up to now, three-metal composite nanoparticles,[28] AuNP-doped metal oxides,[29] and nanomaterials with heterojunction structures[30] have been employed as CRAs for amplifying the ECL signal. The complex structures of these nanomaterial-based CRAs usually result in unsatisfactory

Received: August 14, 2022
Accepted: September 19, 2022
Published: September 30, 2022

https://doi.org/10.1021/acs.analchem.2c03546
Anal. Chem. 2022, 94, 14047−14053

utilization efficiency of active centers and hamper elucidation of the correlation between structures and properties. Thus, it is still a long-pursued goal to develop novel ECL CRAs with higher efficiency and simpler structure.

On account of their atomically dispersed metal active centers, single-atom catalysts (SACs) have been one family of the most attractive catalysts for the ultrahigh utilization efficiency of active centers close to 100%. They play outstanding roles in numerous fields including environmental remediation,[31] organic syntheses,[32] photodynamic therapy,[33] and energy conversion[34] due to their excellent catalytic performance. For most of the application fields, SACs generate abundant ROS to significantly accelerate the reaction procedure. Inspired by the fact, SACs can be a potential powerful signal booster for ECL systems involving participation of ROS.

Typically, SACs are prepared by calcining metal precursors on the carriers to promote the formation and improve stability of atomically dispersed metal active centers.[35−37] However, high-temperature calcination inevitably destroys the hydrophilic groups of SACs and lowers their aqueous dispersibility. Thus, it is a huge challenge to apply SACs as signal probes to tag biorecognition molecules for bioassay although they have displayed high catalytic activity superior to natural enzymes and regular nanomaterials.

As a polymer with abundant hydrophilic groups, PEG can afford ideal aqueous dispersibility to hydrophobic materials. Herein, Ni SACs synthesized by high-temperature calcination of precursors were functionalized with PEG 2000 to obtain PEGylated Ni SACs (Ni@PEG), which retained excellent catalytic performance for ORR. Then, the highly hydrophilic SACs were adopted to develop a sensitive ECL system by utilizing the generated ROS to boost the ECL emission of luminol. To demonstrate their application potential in bioassay, they were used to tag phage recombinant cell-binding domain (CBD) for recognizing MRSA. By adopting porcine IgG to modify glassy carbon electrode (GCE) deposited with gold nanoparticle (AuNP) films, a sensitive biosensor was developed for ECL assay and AST of MRSA.

EXPERIMENTAL SECTION

Preparation of Ni SACs. A high-temperature calcination protocol reported by Zhu's group[38] with slight modifications was applied to synthesize Ni SACs. In brief, 12.4 mg of $Ni(CH_3COO)_2{\cdot}4H_2O$ and 29.7 mg of 1,10-phenanthroline monohydrate were dissolved in 15 mL of ethanol. The solution was added with 69.6 mg of carbon black and stirred at 60 °C for 2 h. Then, the mixture was heated in a rotary evaporator at 50 °C for removing ethanol. The product was grinded and heated to 600 °C at a rate of 5 °C/min and then reacted for 2 h in argon atmosphere. For comparison, N−C was prepared with the a similar protocol without addition of $Ni(CH_3COO)_2{\cdot}4H_2O$.

Preparation of Ni@PEG. Two milligrams of Ni SACs and an equal amount of NH_2−PEG(2000)−COOH were dispersed into 2.0 mL of water and sonicated in an ice bath for 1 h (sonication for 3 s, pause for 7 s) with an ultrasonic homogenizer at a power of 60 W. After washing thrice, the suspension of Ni@PEG was stored at 4 °C till use.

Preparation of CBD. The detailed experimental procedures for preparing CBD are described in the Supporting Information. In brief, *Escherichia coli* (*E coli*) transformed with CBD plasmid was induced to express the target protein. After ultrasonic disruption of *E coli* cells, the supernatant containing CBD was collected and purified with nickel affinity chromatography to obtain the target protein with high purity.

Preparation of Ni@PEG-CBD. One milliliter of Ni@PEG suspension at 1.0 mg/mL was activated with 20 mg of EDC and 5 mg of NHS for 20 min. Then, it was added with 50 μL of CBD solution at 0.5 mg/mL. After 12 h reaction at 4 °C, the product of Ni@PEG-CBD was washed to remove unreacted CBD, re-dispersed into 2.0 mL of PBS, and stored at 4 °C until use.

Conjugation of Fluorescent Dyes with Proteins. One milliliter of protein solution at 1.0 mg/mL was mixed with 500 μL of fluorescent dye solution at 2.0 mg/mL. After 2 h conjugation at 37 °C, the product was dialyzed against PBS for 24 h to remove unconjugated dyes. With such a protocol, the conjugates of porcine IgG-Rhodamine B isothiocyanate (RBITC) and CBD-FITC were prepared.

Fabrication of ECL Biosensor. A GCE (Φ = 3 mm) was polished and cleaned before modification. Then, the GCE was treated with a constant potential of −0.20 V for 120 s in 2.0 mL of $HAuCl_4$ solution at 20.0 mM to deposit AuNP films. The AuNP film-deposited GCE was modified with 5.0 μL of porcine IgG at 40 μg/mL for 12 h at 4 °C and blocked with 1% BSA for 1 h at 37 °C.

ECL Assay of MRSA. The biosensor was incubated with 100 μL of MRSA sample at 37 °C for 1 h and then with 5.0 μL of Ni@PEG-CBD at 0.5 mg/mL for 45 min. After flush, it was immersed into 4.0 mL of CBS buffer (50.0 mM, pH 9.6) added with 200 μL of luminol at 0.10 mM. Then, it was scanned from −0.60 to 0.60 V at a speed of 0.20 V/s to collect the ECL signal.

AST of MRSA. Four antibiotics including vancomycin (VAN), rifampicin (RIF), clindamycin (CLI), and azithromycin (AZM) were adopted to test the susceptibility of MRSA. In detail, 100 μL of antibiotic solution was used to treat the equal volume of bacterial culture at 7.3×10^3 CFU/mL prepared in MH II broth for 1.5 h at 37 °C. With the ECL biosensor, the signal produced by MRSA was collected to determine the minimal inhibitory concentration (MIC) values of the antibiotics. For comparison, the broth microdilution protocol described in CLSI document M100 was also adopted to acquire their MIC values.

RESULTS AND DISCUSSION

Characterization of Ni SACs. By using 1,10-phenanthroline and Ni ions as precursors, atomically dispersed Ni was prepared on the carrier of carbon black by a high-temperature calcination protocol. The TEM photograph reveals that Ni SACs are particles smaller than 50 nm (Figure 1A). Just unordered lattice fringes of carbon black can be observed in the high-resolution TEM photograph (Figure S1), indicating the absence of Ni aggregates. As revealed in the aberration-corrected high-angle annular dark-field scanning transmission electron microscopy (AC HAADF-STEM) photograph, numerous bright dots are evidently dispersed on the carbon black (Figure 1B), confirming the presence of atomically dispersed Ni element. X-ray absorption near-edge structure (XANES) and X-ray absorption fine structure (EXAFS) spectra were measured at the Ni K edge to study the structure of Ni SACs at the atomic level. The energy absorption edge of Ni SACs is positioned between those of Ni foil and NiO (Figure 1C), suggesting that Ni element is positively charged and the valence state does not exceed +2. Figure 1D shows an

https://doi.org/10.1021/acs.analchem.2c03546
Anal. Chem. 2022, 94, 14047−14053

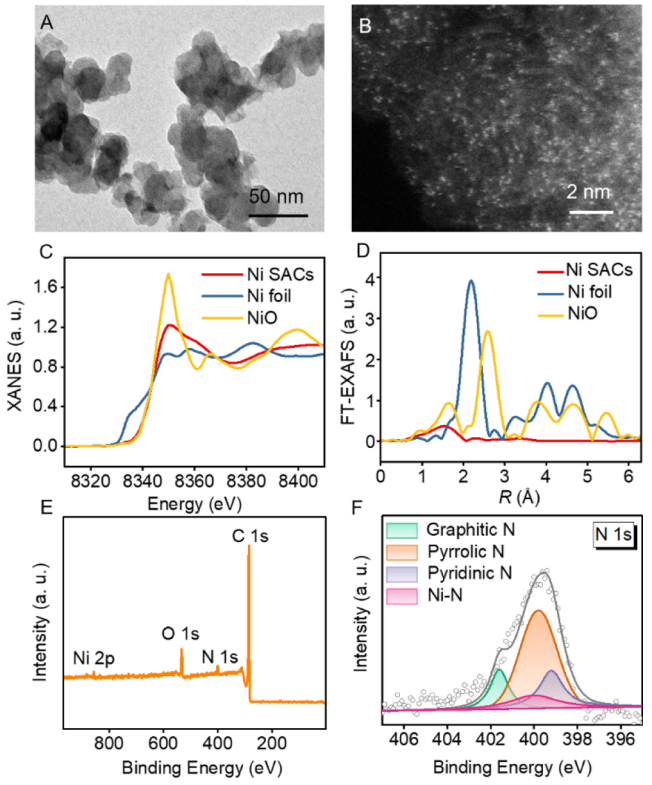

Figure 1. (A) TEM photograph of Ni SACs. (B) AC-HAADF-STEM photograph of Ni SACs. (C) Normalized XANES spectra of Ni SACs, Ni foil, and NiO. (D) FT-EXAFS plots at Ni K edge of Ni SACs, Ni foil, and NiO. (E) Full XPS pattern of Ni SACs. (F) N 1s XPS pattern of Ni SACs.

EXAFS peak for Ni SACs at 1.48 Å, which is the initial coordination shell of Ni−N bond.[38] Furthermore, the peaks for Ni−Ni bond (2.20 Å) and Ni−O (1.61 Å) bond are not observed, also suggesting the absence of Ni and NiO aggregates. Therefore, atomically dispersed Ni element is believed to coordinate with N element. In order to acquire the specific coordination number, the EXAFS of Ni SACs was fitted sequentially in k and R spaces using $E-k$ conversion and Fourier transform (Figure S2). As summarized in Table S1, each Ni atom coordinated with four N atoms, and the bond length is 2.04 Å.

According to the results of energy dispersive spectroscopy elemental mapping, Ni SACs are composed of Ni, N, C, and O elements (Figure S3), consistent with the XPS data shown in Figures 1E,F and S4. Furthermore, the loading amount of Ni atoms in Ni SACs was measured to be 2.06 wt % by an ICP-emission spectrometer. As shown in Figure S5, the XRD pattern of Ni SACs is in conformity with that of N−C, in which only (002) and (100) crystal planes of graphite are observed. Therefore, there is no Ni-based crystal phase. The structural detail of carbon black was investigated by Raman spectroscopy. Figure S6 shows a peak at 1596 cm^{-1} (graphite sp^2 carbon) and a peak at 1344 cm^{-1} (disordered sp^3 carbon), which correspond to G and D bands, respectively.[39] The I_D/I_G ratio of Ni SACs is 1.39, while that of N−C is 1.04. Therefore, Ni SACs possess abundant defects, which facilitate the adsorption of dissolved oxygen on the active sites of Ni SACs for ORR, resulting in greatly improved catalytic performance.

ECL Catalytic Behavior and Mechanism of Ni SACs. The ECL enhancement effects of N−C and Ni SACs on luminol system were studied in nitrogen-saturated, air-saturated, and oxygen-saturated solutions. Figure S7 shows that the ECL signal emitted from GCE modified with 5.0 μL of N−C suspension (1.0 mg/mL) in the nitrogen-saturated solution was quite weak. Even after the luminol solution was bubbled with air and oxygen to achieve saturation state, the ECL signals increased only by 2.6 and 3.5 times, respectively. However, for GCE modified with an equal amount of Ni SACs,

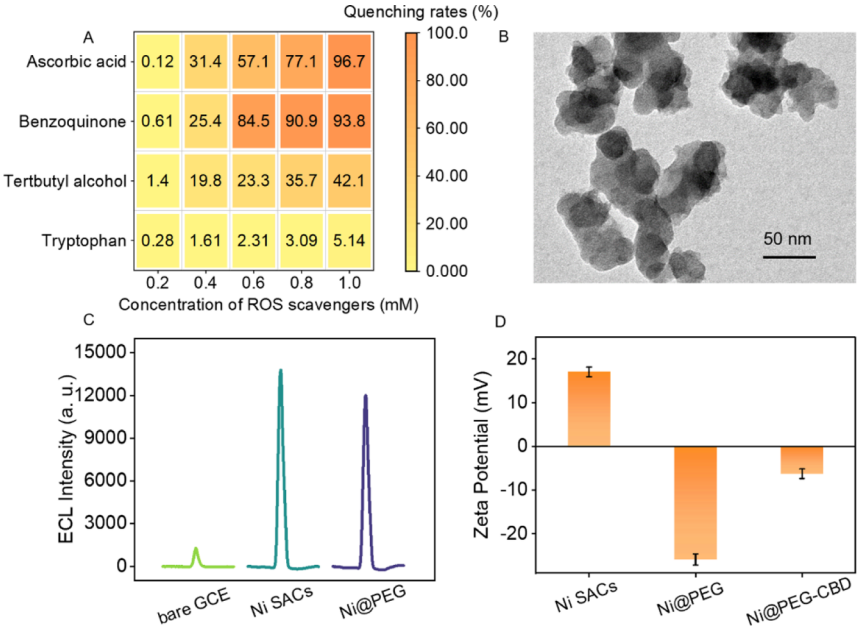

Figure 2. (A) Quenching rates of ECL signal emitted from Ni SACs modified GCE with addition of diverse ROS scavengers. (B) TEM photograph of Ni@PEG. (C) ECL signals emitted from bare GCE, GCE modified with Ni SACs, and Ni@PEG. (D) Zeta potential of Ni SACs, Ni@PEG, and Ni@PEG-CBD.

https://doi.org/10.1021/acs.analchem.2c03546
Anal. Chem. 2022, 94, 14047−14053

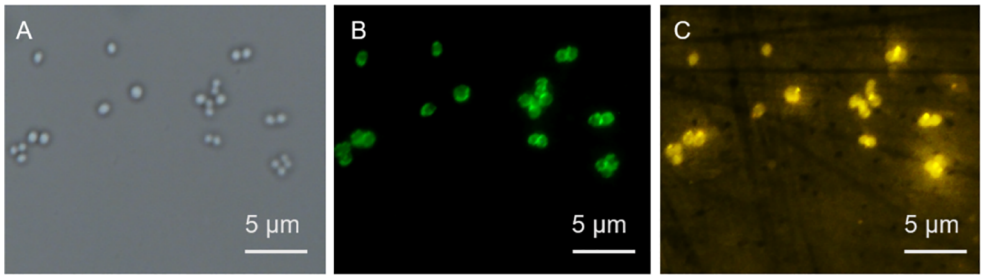

Figure 3. Fluorescent micrographs of MRSA stained with FITC-CBD and RBITC-porcine IgG: (A) bright field, (B) green fluorescence channel, and (C) yellow fluorescence channel.

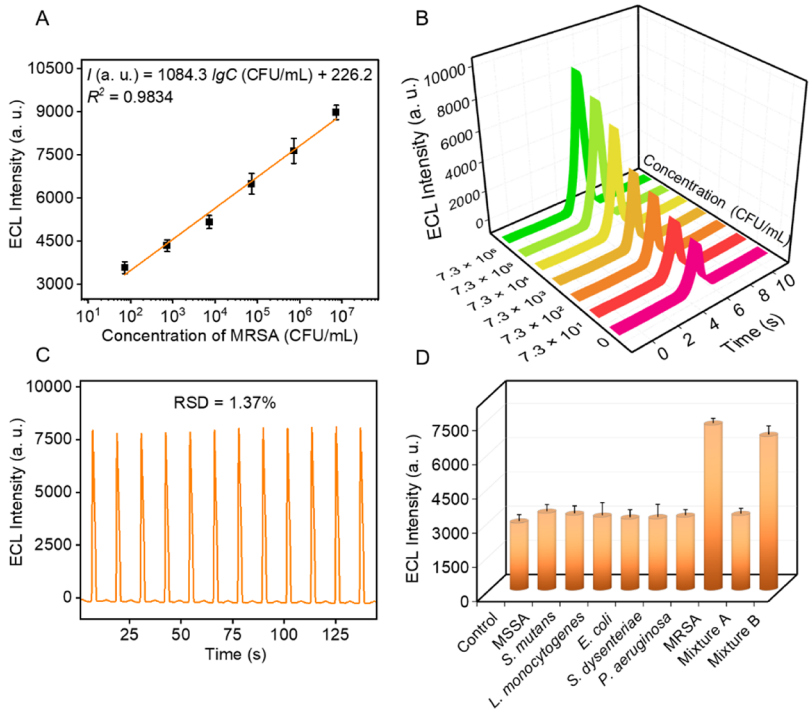

Figure 4. (A) Regressive curve for ECL assay of MRSA, $n = 3$. (B) ECL signals of MRSA at diverse concentrations. (C) Stability test of ECL biosensor for 12 cycles of continuous potential scanning. (D) ECL signals of diverse bacteria all at 7.3×10^5 CFU/mL, $n = 3$.

the ECL signals significantly increased by 17.6 and 22.8 times in air-saturated and oxygen-saturated luminol solutions, respectively. Based on the above data, Ni SACs are identified as highly efficient CRAs for the ECL reaction of luminol system, in which Ni atom plays a key role in boosting ECL signal.

Some radical scavengers at diverse concentrations were added into the luminol solution to explore the mechanism of ECL reaction catalyzed by Ni SACs, including ascorbic acid (total ROS scavenger), benzoquinone ($O_2^{\bullet-}$ scavenger), *tert*-butyl alcohol ($OH^{\bullet}$ scavenger), and tryptophan ($^1O_2$ scavenger). As seen in Figure 2A, the ECL emission was quenched by 96.7% after addition of 1.0 mM ascorbic acid, revealing that the ECL signal was triggered by ROS. Meanwhile, benzoquinone and tertbutyl alcohol at an equal concentration also significantly quenched the ECL emission by 93.8 and 42.1%, respectively, implying the participation of $O_2^{\bullet-}$ and $OH^{\bullet}$ in the ECL reaction. The results also suggest that partial $O_2^{\bullet-}$ converted to $OH^{\bullet}$ via a cathodic procedure because the sum of the quenching rates of $O_2^{\bullet-}$ and $OH^{\bullet}$ is higher than 100%. However, with the addition of tryptophan at the equal concentration, the ECL intensity showed minor decrease of 5.14%, implying negligible participation of $^1O_2$.

With the above data, the probable mechanism of the ECL reaction catalyzed by Ni SACs is summarized as follows. As dissolved oxygen diffused to the surface of GCE, it was reduced to $O_2^{\bullet-}$ via cathodic potential scanning with the catalysis of Ni active sites. Meanwhile, partial $O_2^{\bullet-}$ converted to $OH^{\bullet}$ by breaking the O−O bond.[38] Thereafter, luminol anion (LH^-) converted to its radical ($L^{\bullet-}$) via anodic potential scanning. Then, $L^{\bullet-}$ was oxidized by highly active $O_2^{\bullet-}$ and $OH^{\bullet}$ to form excited-state 3-aminophthalic acid anion (AP_2^{2-*}). Lastly, it returned to the ground state, accompanied with intensive emission of ECL signal.

$$O_2 + e^- \rightarrow O_2^{\bullet-}$$

$$O_2^{\bullet-} + H_2O \rightarrow OH^{\bullet} + OH^-$$

$$LH^- - e^- \rightarrow L^{\bullet-} + H^+$$

$$L^{\bullet-} + O_2^{\bullet-} \rightarrow AP_2^{2-*} + N_2$$

$$L^{\bullet-} + OH^{\bullet} \rightarrow AP_2^{2-*} + N_2$$

https://doi.org/10.1021/acs.analchem.2c03546
Anal. Chem. 2022, 94, 14047−14053

$$AP_2^{2-*} \rightarrow AP_2^{2-} + h\nu$$

Properties of Ni@PEG. As shown in Figure S8, Ni SACs without PEG 2000 are hydrophobic, and thus, their precipitates in water were adsorbed onto the wall of glass vial. After Ni SACs were functionalized with PEG 2000, the obtained Ni@PEG became much more hydrophilic and well dispersed in water. Meanwhile, the functionalized SACs kept their original morphology (Figure 2B). In a further study, Ni@PEG was found to enhance the ECL emission of luminol by 15.8 times in the presence of dissolved oxygen, which shows a slight decrease of 10.8% compared with Ni SACs (Figure 2C). The slight signal decrease could be ascribed to the partial isolation of active sites from dissolved oxygen.

Characterization of Ni@PEG-CBD. The SDS-PAGE photograph in Figure S9 reveals that the molecular weight (MW) of CBD was around 13 kDa. The change in zeta potential was measured for proving the successful preparation of Ni@PEG-CBD. As illustrated in Figure 2D, Ni SACs show a positive zeta potential of 17.8 eV. After they were modified by electrostatic adsorption of PEG 2000, the zeta potential decreased to −25.9 eV due to the influence of carboxyl terminus in PEG 2000 molecules. After Ni@PEG was conjugated with CBD, the zeta potential was measured to be −3.89 eV, which is due to the covalent conjugation between surface carboxyl terminus and CBD.

Binding of MRSA and Recognition Molecules. In order to study the binding ability of recognition molecules toward MRSA, the bacterial cells were incubated with RBITC-porcine IgG as well as FITC-CBD and imaged with a fluorescence microscope (experimental procedure provided in the Supporting Information). As shown in Figures 3A−C, both green fluorescence from FITC and yellow fluorescence from RBITC distributed over bacterial surface. The result proves the feasibility of dual-site recognition approach for ECL assay of MRSA. Afterward, MRSA cells were incubated with Ni@PEG-CBD and imaged with a transmission electron microscope. Figure S10 shows that numerous Ni@PEG-CBDs were attached onto the bacterial surface, confirming that the binding activity of CBD was not affected by its covalent conjugation with SACs.

Performance of ECL Biosensor for MRSA. The electrochemical behaviors including CV and EIS were studied to characterize the ECL biosensor as described in the Supporting Information. The results provided as Figure S11 confirm its different stages of fabrication and incubation.

An MRSA standard sample at 7.3×10^3 CFU/mL was used to optimize the analytical conditions. As summarized in Figure S12, porcine IgG at 40 μg/mL was used to fabricate the biosensor, and 60 and 45 min were adopted to incubate the sample and Ni@PEG-CBD, respectively.

With the adopted analytical conditions, MRSA can be quantified within a linear range of $73-7.3 \times 10^6$ CFU/mL, with a correlation coefficient (R^2) of 0.9834 (Figure 4A,B). The detection limit for MRSA was determined to be 25 CFU/mL (3σ). The RSD for 12 cycles of continuous potential scanning is 1.37%, showing good stability (Figure 4C). The biosensor shows superior detection limit and linear range than the previously reported works (Table S2), which can be ascribed to the usage of Ni@PEG as highly sensitive ECL probes.

Selectivity of Biosensor for MRSA. Methicillin-susceptible *S. aureus* (MSSA), *Listeria monocytogenes* (*L. monocytogenes*), *Streptococcus mutans* (*S. mutans*), *Pseudomonas aeruginosa* (*P. aeruginosa*), *E. coli*, and *Shigella dysenteriae* (*S. dysenteriae*) were used as non-target bacteria for testing the selectivity of the ECL biosensor for MRSA. All bacteria are at an equal concentration of 7.3×10^5 CFU/mL in the tests. The values of the interference factor (*IF*) were calculated by eq 1

$$IF = (I_1 - I_0)/(I_2 - I_0) \times 100\% \quad (1)$$

In this equation, I_0, I_1, and I_2 are the ECL signals generated by negative control (PBS), the non-target bacteria, and positive control (MRSA), respectively. As shown in Figure 4D, all these non-target bacteria generated ECL signals close to that of the negative control. The *IF* values of MSSA, *L. monocytogenes*, *S. mutans*, *P. aeruginosa*, *E. coli*, and *S. dysenteriae* are 10.0, 7.9, 5.9, 4.0, 4.2, and 5.9%, respectively. For mixture A, comprising all the six non-target bacteria, the *IF* value is 7.5%. Meanwhile, for mixture B, comprising MRSA and the non-target bacteria, the generated ECL signal is only 7.4% lower than that of MRSA.

Assay of MRSA in Spiked Samples. Some real samples including human urine, physiological saline injection, and human serum were spiked with diverse amounts of MRSA standard samples and assayed with the ECL biosensor. As summarized in Table 1, the recovery values are from 80.8 to 119.2%, and the RSD values are from 2.8 to 9.4%, showing its reliability for assaying real sample.

Table 1. Results of Recovery Tests for Real Samples Spiked with MRSA, $n = 3$

sample	spiked concentration (CFU/mL)	found concentration (CFU/mL)	RSD (%)	recovery (%)
human urine[a]	7.3×10^4	5.9×10^4	3.8	80.8
	7.3×10^5	7.4×10^5	2.8	101.4
	7.3×10^6	7.9×10^6	4.2	108.2
physiological saline injection	7.3×10^4	6.1×10^4	8.9	83.6
	7.3×10^5	6.3×10^5	7.8	86.3
	7.3×10^6	8.7×10^6	2.8	119.2
human serum[b]	7.3×10^4	7.9×10^4	5.0	108.2
	7.3×10^5	6.2×10^5	7.7	84.9
	7.3×10^6	6.6×10^6	9.4	90.4

[a]The sample was diluted 20 times before assay. [b]The sample was diluted 50 times before assay.

AST of MRSA. Four diverse types of antibiotics, including VAN in glycopeptide family, CLI in lincosamide family, RIF in ansamycin family, and AZM in macrolide family, were used to explore the application potential of the ECL biosensor for AST. For a comparison, an MRSA culture without addition of antibiotics was kept at 4 °C for 90 min. At such a low temperature, the bacterial culture kept an almost unchanged concentration due to the extremely low growth speed and thus was used as a control group (CG).

As illustrated in Figure 5, the ECL signal generated by bacterial culture exposed to VAN at 8 μg/mL is 55.0% of that without VAN and does not show significant difference in comparison with that by CG ($p > 0.05$). Thus, the MIC of VAN is determined to be 8 μg/mL. Similarly, the MIC values of CLI and RIF are determined to be 8 and 1 μg/mL, respectively. For AZM, as its concentration reaches 16 μg/mL, the ECL signal of bacterial culture is still 70.9% higher than

https://doi.org/10.1021/acs.analchem.2c03546
Anal. Chem. 2022, 94, 14047−14053

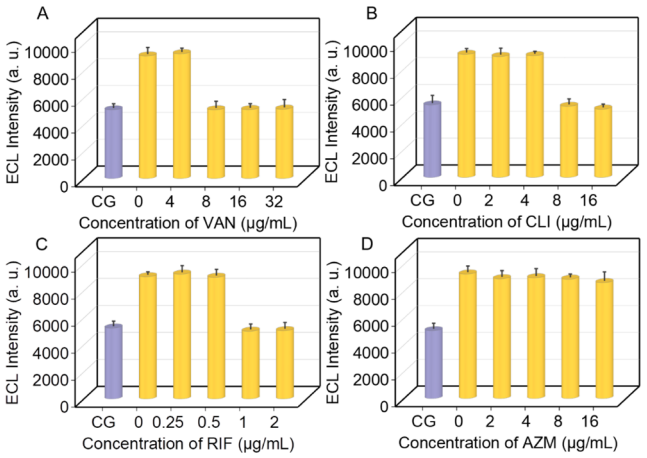

Figure 5. ECL signals of MRSA culture at 7.3 × 10^3 CFU/mL exposed to equal volumes of (A) VAN, (B) CLI, (C) RIF, and (D) AZM at diverse concentrations, n = 3.

that of CG. Thus, its MIC is determined to be > 16 μg/mL. According to the MIC interpretation criteria for MRSA in CLSI M100, 32nd ed (Table S3), the MRSA strain is intermediate resistant to VAN, susceptible to RIF, and resistant to CLI and AZM (Table 2). Meanwhile, the susceptibility of

Table 2. Results of AST of MRSA

	MIC (μg/mL)		
antibiotics	ECL biosensor	broth dilution method	susceptibility
VAN	8	8	intermediate
CLI	8	16	resistant
RIF	1	1	susceptible
AZM	>16	>16	resistant

MRSA to the four antibiotics was also assessed with the conventional broth microdilution technique, and the obtained results are consistent with those by the ECL biosensor.

CONCLUSIONS

In conclusion, a high-temperature calcination protocol was adopted to prepare Ni SACs with outstanding capability for generating ROS through an ORR occurring on cathode. The SACs can act as efficient CRAs to significantly amplify the ECL signal of the luminol system in the presence of dissolved oxygen. To improve their water dispersibility, Ni SACs were functionalized with PEG 2000 to obtain much more hydrophilic Ni@PEG. The carboxyl terminus on the surface facilitates conjugation with recognition molecules. Therefore, the obtained Ni@PEG can be used as ECL probes to achieve a highly sensitive bioassay. In this proof-of-principle work, a biosensor was developed to assay and AST of MRSA in order to prove their application potential. We hope that more SACs materials functionalized with hydrophilic polymers can be developed to meet the demand of sensitive ECL bioassay in the near future.

ASSOCIATED CONTENT

Supporting Information

The Supporting Information is available free of charge at https://pubs.acs.org/doi/10.1021/acs.analchem.2c03546.

Materials; apparatus; preparation of CBD; fluorescent imaging of stained MRSA cells; electrochemical behaviors of ECL biosensor; high-resolution TEM photograph of Ni SACs; Ni K-edge EXAFS fitting curves of Ni SACs; EDS element mapping photographs of Ni SACs; Ni 2p, C 1s, and O 1s XPS patterns of Ni SACs; XRD patterns of Ni SACs and N−C; Raman spectra of Ni SACs and N−C; ECL signals emitted from GCEs modified with N−C and Ni SACs; Photographs of Ni SACs and Ni@PEG dispersed in water; SDS-PAGE photograph of expressed CBD; TEM photograph of Ni@PEG-CBD attached onto the surface of MRSA; CV and EIS characterizations; influences of source of IgG, concentration of porcine IgG, incubation time of MRSA, and incubation time of Ni@PEG-CBD on ΔECL intensity; structural details of Ni SACs extracted from EXAFS fitting; comparison of assay performance of diverse assay methods for MRSA; and MIC interpretation criteria for MRSA (PDF)

AUTHOR INFORMATION

Corresponding Authors

Yong He − *Department of Pharmacy, Affiliated Hospital of Zunyi Medical College, Zunyi 563000, China*; Email: heyongzmu@163.com

Zhifeng Fu − *The State Key Lab of Silkworm Genome Biology, College of Pharmaceutical Sciences, Southwest University, Chongqing 400715, China*; orcid.org/0000-0002-8238-7987; Email: fuzf@swu.edu.cn

Authors

Yuchan Ma − *The State Key Lab of Silkworm Genome Biology, College of Pharmaceutical Sciences, Southwest University, Chongqing 400715, China*

Yu Zhang − *The State Key Lab of Silkworm Genome Biology, College of Pharmaceutical Sciences, Southwest University, Chongqing 400715, China*

Jiaqi Gao − *The State Key Lab of Silkworm Genome Biology, College of Pharmaceutical Sciences, Southwest University, Chongqing 400715, China*

Hui Ouyang − *The State Key Lab of Silkworm Genome Biology, College of Pharmaceutical Sciences, Southwest University, Chongqing 400715, China*

Complete contact information is available at: https://pubs.acs.org/10.1021/acs.analchem.2c03546

Notes

The authors declare no competing financial interest.

ACKNOWLEDGMENTS

This research was funded by the National Natural Science Foundation of China (22074123 and 21964023) and Science and Technology Foundation of Guizhou Province (20201Y044).

REFERENCES

(1) Suea-Ngam, A.; Howes, P.; deMello, J. *Chem. Sci.* **2021**, *12*, 12733−12743.

(2) Chang, C. M.; Chern, J.; Chen, M. Y.; Huang, K. F.; Chen, C. H.; Yang, Y. L.; Wu, S. H. *J. Am. Chem. Soc.* **2015**, *137*, 267−275.

(3) Larsen, J.; Stegger, M.; Andersen, P. S.; Petersen, A.; Larsen, A. R.; Westh, H.; Agersø, Y.; Fetsch, A.; Kraushaar, B.; Käsbohrer, A.; Feβler, A. T.; Schwarz, S.; Cuny, C.; Witte, W.; Butaye, P.; Denis, O.;

Haenni, M.; Madec, J. Y.; Jouy, E.; Laurent, F.; Battisti, A.; Franco, A.; Alba, P.; Mammina, C.; Pantosti, A.; Monaco, M.; Wagenaar, J. A.; de Boer, E.; van Duijkeren, E.; Heck, M.; Domínguez, L.; Torres, C.; Zarazaga, M.; Price, L. B.; Skov, R. L. *Clin. Infect. Dis.* **2016**, *63*, 1349−1352.
(4) Thomas-White, K.; Forster, S. C.; Kumar, N.; Van Kuiken, M. V.; Putonti, C.; Stares, M. D.; Hilt, E. E.; Price, T. K.; Wolfe, A. J.; Lawley, T. D. *Nat. Commun.* **2018**, *9*, 1557.
(5) Loesche, W. J.; Lopatin, D. E.; Stoll, J.; van Poperin, N.; Hujoel, P. P. *J. Clin. Microbiol.* **1992**, *30*, 418−426.
(6) Lazcka, O.; Campo, F. J. D.; Muñoz, F. X. *Biosens. Bioelectron.* **2007**, *22*, 1205−1217.
(7) Schoepp, N. G.; Khorosheva, E. M.; Schlappi, T. S.; Curtis, M. S.; Humphries, R. M.; Hindler, J. A.; Ismagilov, R. F. *Angew. Chem., Int. Ed.* **2016**, *55*, 9557−9561.
(8) Kang, T. S. *Food Chem.* **2019**, *271*, 1−8.
(9) Ottesen, E. A.; Hong, J. W.; Quake, S. R.; Leadbetter, J. R. *Science* **2006**, *314*, 1464−1467.
(10) He, Y. X.; Ren, Y. R.; Guo, B.; Yang, Y. F.; Ji, Y. W.; Zhang, D. H.; Wang, J. L.; Wang, Y. R.; Wang, H. *Food Chem.* **2020**, *310*, 125942.
(11) Li, Y. X.; Xie, G. M.; Qiu, J. H.; Zhou, D. D.; Gou, D.; Tao, Y. Y.; Li, Y.; Chen, H. *Sens. Actuators, B* **2018**, *258*, 803−812.
(12) Yang, H. L.; Wang, Y. R.; Liu, S. Y.; Ouyang, H.; Lu, S. G.; Li, H. T.; Fu, Z. F. *Biosens. Bioelectron.* **2021**, *182*, 113189.
(13) Kong, W. J.; Xiong, J.; Yue, H.; Fu, Z. F. *Anal. Chem.* **2015**, *87*, 9864−9868.
(14) Wang, Y. R.; He, Y.; Bhattacharyya, S.; Lu, S. G.; Fu, Z. F. *Anal. Chem.* **2020**, *92*, 3340−3345.
(15) Pu, G.; Zhang, D.; Mao, X.; Zhang, Z.; Wang, H.; Ning, X.; Lu, X. *Anal. Chem.* **2018**, *90*, 5272−5279.
(16) Richter, M. M. *Chem. Rev.* **2004**, *104*, 3003−3036.
(17) Qi, H. L.; Zhang, C. X. *Anal. Chem.* **2020**, *92*, 524−534.
(18) Tokel, N. E.; Bard, A. J. *J. Am. Chem. Soc.* **1972**, *94*, 2862−2863.
(19) Liu, Y.; Chen, X. Q.; Ma, Q. *Biosens. Bioelectron.* **2018**, *117*, 240−245.
(20) Li, X. J.; Du, Y.; Wang, H.; Ma, H. M.; Wu, D.; Ren, X.; Wei, Q.; Xu, J. J. *Anal. Chem.* **2020**, *92*, 12693−12699.
(21) Zhang, G. Y.; Chai, H. N.; Tian, M. W.; Zhu, S. F.; Qu, L. J.; Zhang, X. J. *Anal. Chem.* **2020**, *92*, 7354−7362.
(22) Cao, W. W.; Liu, L. L.; Yuan, R.; Wang, H. J. *Biosens. Bioelectron.* **2022**, *214*, 114506.
(23) Jiang, X.; Wang, Z.; Wang, H.; Zhuo, Y.; Yuan, R.; Chai, Y. *Chem. Commun.* **2017**, *53*, 9705−9708.
(24) Wang, L.; Jiang, M. H.; Chai, Y. Q.; Yuan, R.; Zhuo, Y. *Chem. Commun.* **2020**, *56*, 9000−9003.
(25) Zou, R.; Xie, R. Y.; Peng, Y. G.; Guan, W. J.; Lin, Y. J.; Lu, C. *Anal. Chem.* **2022**, *94*, 4813−4820.
(26) Guo, J. N.; Xie, M. S.; Du, P. Y.; Liu, Y.; Lu, X. Q. *Anal. Chem.* **2021**, *93*, 10619−10626.
(27) Zong, L. P.; Li, J. J.; Shu, G. F.; Liu, X. Y.; Marks, S.; Cosnier, X. J.; Shan, S.; Shan, D. *Anal. Chem.* **2022**, *94*, 1325−1332.
(28) Wu, F. F.; Zhou, Y.; Zhang, H.; Yuan, R.; Chai, Y. Q. *Anal. Chem.* **2018**, *90*, 2263−2270.
(29) Zhang, X.; Li, W.; Zhou, Y.; Chai, Y.; Yuan, R. *Biosens. Bioelectron.* **2019**, *135*, 8−13.
(30) Yang, L.; Jia, Y.; Wu, D.; Zhang, Y.; Ju, H.; Du, Y.; Ma, H.; Wei, Q. *Anal. Chem.* **2019**, *91*, 14066−14073.
(31) Zhang, N.; Ye, C.; Yan, H.; Li, L.; He, H.; Wang, D.; Li, Y. *Nano Res.* **2020**, *13*, 3165−3182.
(32) Li, W. H.; Yang, J. R.; Wang, D. S.; Li, Y. D. *Chem* **2022**, *8*, 119−140.
(33) Xiang, H.; Feng, W.; Chen, Y. *Adv. Mater.* **2020**, *32*, 1905994.
(34) Wang, Y. C.; Chu, F. L.; Zeng, J.; Wang, Q. J.; Naren, T. Y.; Li, Y. Y.; Cheng, Y.; Lei, Y. P.; Wu, F. X. *ACS Nano* **2021**, *15*, 210−239.
(35) Qu, Q. Y.; Ji, S. F.; Chen, Y. J.; Wang, D. S.; Li, Y. D. *Trends Chem.* **2021**, *3*, 954−968.
(36) Li, L. B.; Huang, B. Y.; Tang, X. N.; Hong, Y. S.; Zhai, W. J.; Hu, T.; Yuan, K.; Chen, Y. W. *Adv. Funct. Mater.* **2021**, *31*, 2103857.
(37) Tong, M. M.; Wang, L.; Fu, H. G. *Small Methods* **2021**, *5*, 2100865.
(38) Gu, W. L.; Wang, X. S.; Wen, J.; Cao, S. Y.; Jiao, L.; Wu, Y.; Wei, X. Q.; Zheng, L. R.; Hu, L. Y.; Zhang, L. Z.; Zhu, C. Z. *Anal. Chem.* **2021**, *93*, 8663−8670.
(39) Fei, H.; Dong, J.; Feng, Y.; Allen, C. S.; Wan, C.; Volosskiy, B.; Li, M.; Zhao, Z.; Wang, Y.; Sun, H.; An, P.; Chen, W.; Guo, Z.; Lee, C.; Chen, D.; Shakir, I.; Liu, M.; Hu, T.; Li, Y.; Kirkland, A. I.; Duan, X.; Huang, Y. *Nat. Catal.* **2018**, *1*, 63−72.

https://doi.org/10.1021/acs.analchem.2c03546
Anal. Chem. 2022, 94, 14047−14053